

# Multi-component seismic-resolution analysis using finite-difference acquisition modelling

**Shaun Strong**  
Velseis Pty Ltd  
sstrong@velseis.com

**Steve Hearn**  
Velseis Pty Ltd and  
University of Queensland  
steveh@velseis.com

## SUMMARY

Various rules-of-thumb (e.g. Fresnel Radius, Rayleigh Limit) are commonly used to predict seismic resolution, based on image wavelength. However, seismic resolution ultimately depends on more fundamental parameters including survey design, source bandwidth, geology and data processing. A more instructive analysis is possible via numerical modelling of the acquisition process. Here we demonstrate the improved insight available with this approach, with examples taken from the coal and petroleum sectors.

We use viscoelastic finite-difference modelling to simulate 2D multi-component acquisition sequences. The ability to allow for anelastic attenuation is important as it permits a more realistic comparison of the resolution achievable on P-wave and PS-wave imagery.

Analysis of a typical coal target suggests that barren-zones of width 5-10 metres can be resolved. The interplay of wavelength and attenuation is such that the PS-wave image is likely to exhibit comparable, or slightly reduced, lateral resolution where statics are not a problem. Resolution can be downgraded significantly if statics are more severe, and in practice this is likely to have greater impact on the PS image.

A second example examines detection of lens-like features at petroleum depth. The resolving ability on the P-wave imagery is broadly consistent with analytical predictions (100m laterally and 40 m vertically). In terms of resolution, the PS-images are perhaps less competitive than at the coal scale, because the longer path lengths yield greater relative attenuation.

Realistic numerical modelling, simulating the full acquisition and processing sequence, leads to a more pragmatic understanding of seismic resolution issues. It is a valuable tool for survey planning and image interpretation.

**Key words:** modelling, multi-component, resolution

## INTRODUCTION

A number of simple rules-of-thumb have been widely used to predict vertical and horizontal resolution limits (e.g. Rayleigh and Widess limits; Fresnel radius (see e.g. Sheriff, 1999; Lindsey, 1989)). Such indicators have been extended via more recent analytical studies. For example, Chen and Schuster

(1999) provide expressions to predict the resolution achievable with migrated data. These measures all provide valuable insight into the relationship between final image-wavelength and resolution. However, seismic resolution ultimately depends on more fundamental factors. These include survey design (fold, receiver spacing, aperture etc.), source bandwidth, geology, and the design and sequence of algorithms used in the CMP stacking process. As targets become more subtle, resolution analysis needs to be more controllable in terms of these individual factors.

The idea of extending understanding of resolution via modelling is not new. Hilterman (1982) carried out a range of zero-offset resolution modelling exercises, and schemes with increasing sophistication have evolved since. For this investigation we use viscoelastic finite-difference modelling (e.g. Robertsson et al., 1994) to simulate the acquisition of a sequence of multi-component shot records over 2D geological models of arbitrary complexity. These shot records are then processed and interpreted using standard real-data methods. This provides the ability to compare different processing algorithms with respect to resolution.

Attenuation ( $Q$ ) is specified throughout the model for P-waves and S-waves independently. This allows instructive examination of the competing effects of shorter wavelength, but increased attenuation, for S waves, and permits comparison of the resolution capabilities of conventional and converted-wave (PS-wave) images.

## COAL-SCALE EXAMPLE

Table 1 presents a number of useful analytical indicators of lateral resolution, for coal-scale targets at different depths. As an example, we will consider the target at 150m depth in some detail. Columns 2-4 give Fresnel radii for P waves, and for PS waves under different frequency assumptions. These numbers can be considered as indicative of lateral resolution on unmigrated data, and have been primarily used to assess the relative resolution of P and PS data. If the dominant frequencies on P and PS images were comparable, we would expect shorter wavelengths, and hence better resolution on PS-wave images (Fresnel radius = 25m) than on P-wave images (Fresnel radius = 59m). However, our experience with PS-wave coal reflection suggests that the dominant frequency on the PS image may often be only half that on the P image. On this practical assumption, the Fresnel radius (65m) would imply slightly reduced resolving power for PS compared to P. The analytical analysis of Chen and Schuster (1999) predicts that the expected resolution on the migrated P-wave image would be about 12m, and by extension therefore slightly greater on the PS image.

**Table 1. Analytical indicators of lateral resolution for coal targets at different depths.**

Depth	Fresnel Radius (P)	Fresnel Radius (PS)		Resolution After Migration (P)
		$f_{PS} = f_P$	$f_{PS} = f_P/2$	
50	34	26	37	4
100	48	37	53	8
<b>150</b>	<b>59</b>	<b>46</b>	<b>65</b>	<b>12</b>
200	68	53	75	15
250	76	59	84	19

Acquisition modelling provides the opportunity to explore the validity of these analytical predictors, and to gain deeper insight regarding underlying causal influences on resolution. We will illustrate the concept with reference to a target coal seam at a depth of 150m, and interrupted by so-called barren zones of various dimensions (Figure 1). A realistic 2D acquisition sequence has been simulated, with shot records constructed via the viscoelastic finite-difference approach. In the initial exercise,  $Q_P$  and  $Q_S$  have been made equal throughout the model, a reasonable starting assumption (e.g. Toksoz et al, 1979). A standard processing sequence has been used. To examine the influence of statics, the modelling process has been carried out for a model with constant weathering, and then for the same model but with a realistic weathering profile, as shown in Figure 1. For reference, the resultant migrated P and PS images for the two cases are included in the Appendix (Figure A1).

A useful means of assessing lateral resolution is via a simple amplitude attribute, derived over the target coal seam. Figure 2 summarises this attribute for the P and PS images, with and without statics interference. In the absence of statics, the P-wave attribute (red) can easily detect the barren zone of width 10m, and can arguably detect the 5m feature. Where statics are present and uncorrected (green) they can introduce attribute variations similar in scale to the geological features. Fortunately, P-wave static algorithms are generally reliable, so that in practice the risk of such spurious attribute anomalies is not high.

In the absence of statics, the PS-wave attribute (blue) shows slightly poorer resolution than P, being just unable to resolve the 5m feature. The PS-wave attribute is much more susceptible to statics effects (magenta) such that reliable detection of features narrower than 20m would be problematic. In general, PS-wave statics solution is more difficult than for P (e.g. Meulenbroek and Hearn, 2007), and hence the risk of degraded resolution is greater.

Finally, note that for this coal-scale example, in the absence of extreme attenuation and static errors, both the P and PS images show better resolution than predicted analytically by Chen and Schuster (1999).

These broad conclusions regarding lateral resolution are consistent with observed changes in spectral bandwidth over the target horizon. Figure 3 illustrates that the P-wave images with (green) and without (red) statics exhibit similar bandwidths. (The slight increase in spectral character in the absence of statics (red) relates to the spectral periodicity introduced when the base-of-seam reflector is better defined.)

The spectra provide interesting insight into the interplay between S-wave wavelength and anelastic attenuation, in controlling the relative resolution on the PS image. Firstly, consider the case where the weathering is constant (no static variations) and where  $Q_P = Q_S$  throughout the model. In this situation, the PS spectrum (blue) exhibits slightly reduced dominant frequency, and bandwidth, compared to the P-wave spectrum (red). Even though  $Q$  values are the same, the PS-waves suffer higher attenuation since the path contains more cycles than for P. This effect is sufficient to cancel the potential resolution advantage attached to the lower velocity (and hence shorter wavelength) of S-waves.

The spectra also emphasise the potentially damaging effects of uncorrected statics (magenta curve) on PS resolution. The effect on bandwidth is significant. For example, in the absence of statics, all  $Q_S$  values would need to be reduced to  $2/3 Q_P$  to produce a similar bandwidth reduction (yellow curve).

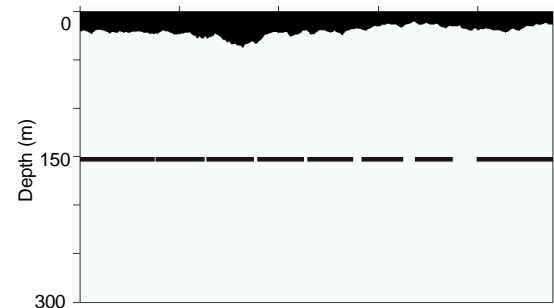


**Figure 1. Coal scale model with a weathering layer of varying depth. The target coal seam is at 150m and includes barren zones having widths of 5, 10, 15, 20, 40, 60, and 120m. A realistic  $Q$  model has been used with  $Q_P = Q_S$  throughout the model.**

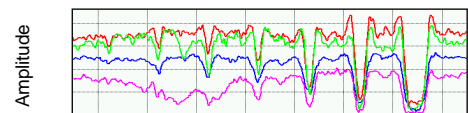


**Figure 2. Amplitude attribute corresponding to the coal reflector in Figure 1, and developed from the sections in Figure A1. P-wave, constant weathering thickness, red; P-wave, variable weathering thickness, green; PS-wave, constant weathering thickness, blue; PS-wave, variable weathering thickness, magenta. Low amplitude responses can be attributed to barren zones or mis-stacking associated with static errors. The barren zones have widths of 5, 10, 15, 20, 40, 60, and 120m respectively.**

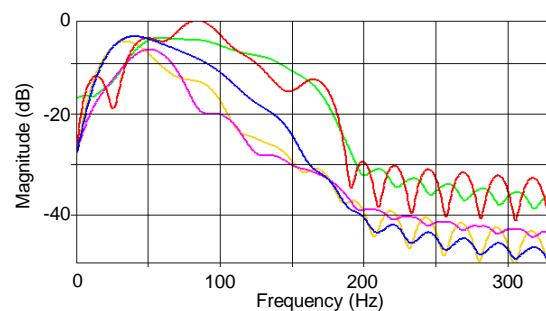


**Figure 3. Magnitude spectra about the coal reflector. P-wave, constant weathering thickness, red; P-wave, variable weathering thickness, green; PS-wave, constant weathering thickness, blue; PS-wave, variable weathering thickness, magenta; PS-wave, constant weathering thickness and  $Q_S = 2/3 Q_P$ , yellow.**

### PETROLEUM SCALE EXAMPLE

Table 2 gives analytical indicators of lateral resolution for targets at various depths. Consider, for example, a target at 1850m depth. If the dominant frequency on the PS image were comparable with that on the P image, then the Fresnel radius would be smaller (288m) on the PS image than on the P image (370m). In reality, even for similar Q values, attenuation leads to reduced dominant frequency on PS, and hence the Fresnel radius is likely to be greater than for P (407m). The Chen and Schuster analysis suggests that lateral resolution on a migrated P-wave image is of order 90m, which implies a value slightly greater than this for the PS image.

**Table 2. Analytical indicators of lateral resolution for petroleum targets at different depths.**

Depth	Fresnel Radius (P)	Fresnel Radius (PS)		Resolution After Migration (P)
		$f_{PS}=f_P$	$f_{PS}=f_P/2$	
1600	344	268	379	79
<b>1850</b>	<b>370</b>	<b>288</b>	<b>407</b>	<b>91</b>
2100	394	307	434	104
2350	417	325	459	116

Figure A2 (Appendix) shows a petroleum-scale model incorporating stylised sand-lenses of decreasing dimension, at a target depth of 1850m. The P-wave and PS-wave images derived through the modelling process are also shown. Close examination of the P-wave images (Figure A2 (b)) suggests that we can detect values smaller than 100m, although these lose definition and are difficult to characterize. This essentially supports the Chen and Schuster prediction of about 90m lateral resolution. Examination of the PS images (Figure A2 (c)) supports the notion that the PS lateral resolution is slightly poorer than on the P images.

We can also examine vertical resolution on this model. Table 3 shows analytical indicators of vertical resolution for the target at depth 1850m. Careful examination of the P-wave image in Figure A2 (b) indicates that the top and bottom interfaces of the feature are defined for the vertical dimension of 60m, but not quite for a vertical dimension of 30m. This suggests that the Rayleigh limit (40m) in this case provides a valid estimate of vertical resolution. Table 3 also indicates that the corresponding Rayleigh Limit for PS would be about 50m, again assuming that PS dominant frequency were half that for P. Examination of the PS images in Figure A2 (c) indicates that the top and bottom faces are just distinguishable for a separation of 60m, confirming the rule-of-thumb prediction.

**Table 3. Analytical indicators of vertical resolution for petroleum target at a depth of 1850m.**

P Wavelength ( $\lambda$ )	160 m
Rayleigh resolution limit ( $\lambda/4$ )	40 m
Widess limit ( $\lambda/8$ )	20 m
Detectable limit ( $\lambda/30$ )	5 m
PS scale factor ( $f_{PS}=f_P$ )	0.61
PS scale factor ( $f_{PS}=f_P/2$ )	1.21

Spectral analysis (Figure 4) of the modelled images further quantifies the relative performances of P and PS, in terms of lateral and vertical resolution. Even though  $Q_P=Q_S$  throughout the model, the PS spectrum is significantly more attenuated than P, since the path contains more cycles. The PS spectrum indicates a dominant frequency about half that for P, consistent with our working assumption. Overall, however, the PS spectrum is attenuated more severely, relative to P, than in the coal example.

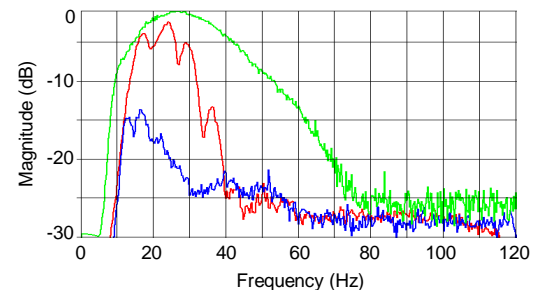


**Figure 4. Magnitude spectra for the 1000x300m sand lens given in Figure A2 (Appendix). Source spectrum, green; P-wave spectrum, red; PS-wave spectrum, blue.**

### CONCLUSIONS

Realistic numerical modelling, simulating the full acquisition and processing sequence, provides valuable insight into resolution issues. It augments analytical rules of thumb, and is a valuable tool for survey planning and image interpretation.

In this paper we have demonstrated resolution issues for representative coal and petroleum scale models, including barren-zones and sand lenses. These examples quantify conventional P-wave resolution capabilities, and also clarify the various issues which restrict PS-wave resolution, particularly in the petroleum context.

### ACKNOWLEDGMENTS

Our processing software is developed within the framework of Seismic Unix, from Colorado School of Mines.

### REFERENCES

- Chen, J. and Schuster, G.T., 1999, Resolution limits of migrated images: *Geophysics*, 64, 1046-1053.
- Hilterman, F.J., 1982, Interpretive lessons from three-dimensional modeling: *Geophysics*, 47, 784-808.
- Lindsey, J.P., 1989, The Fresnel zone and its interpretive significance: *Geophysics: The Leading Edge of Exploration*, 8 (10), 33-39.
- Meulenbroek, A. and Hearn, S., 2007, Analysis of converted refractions for shear statics. 19th ASEG Conference, Perth.
- Robertsson, J., Blanch, J., Symes, W., 1994, Viscoelastic finite-difference modeling: *Geophysics*, 59, 1444-1456.
- Sheriff, R.E., 1999. *Encyclopedic Dictionary of Exploration Geophysics* 3rd Ed. Oklahoma.
- Toksoz, M.N., Johnston, D.H., Timur, A., 1979, Attenuation of seismic waves in dry and saturated rocks: 1. Laboratory measurements: *Geophysics*, 44, 681-690.

APPENDIX

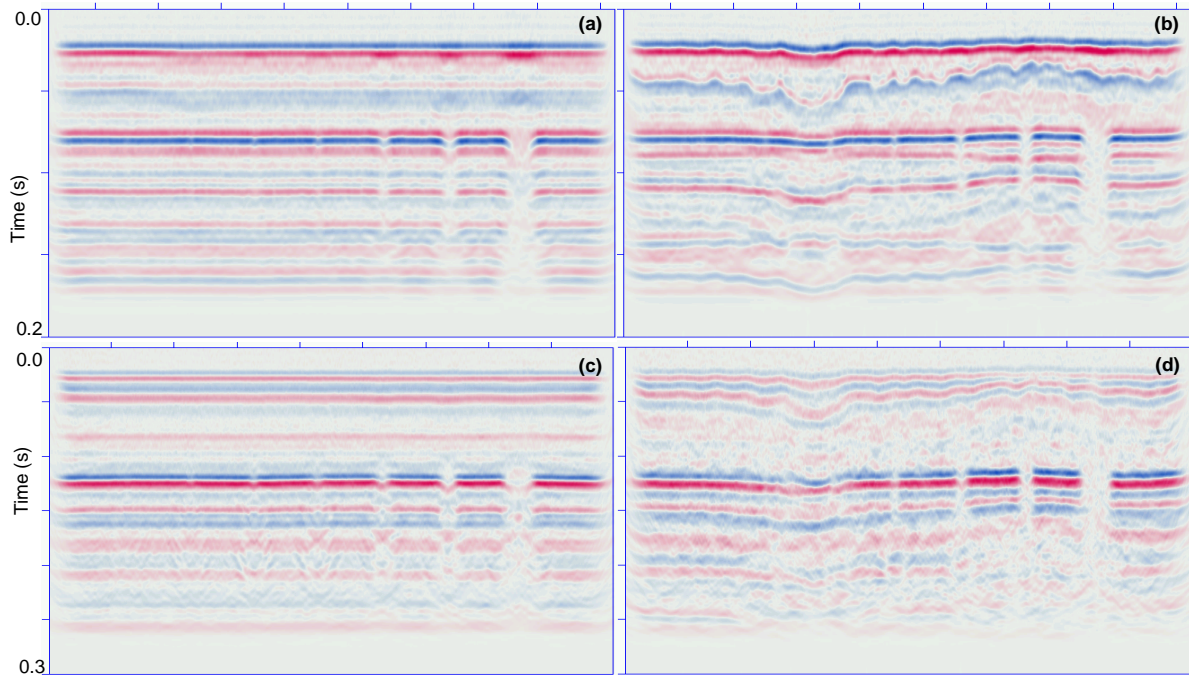


Figure A1. Post-stack migrated sections for the coal-scale example. The target coal seam includes barren zones of widths 5, 10, 15, 20, 40, 60, and 120m corresponding to the model in Figure 1. (a) P-wave, constant weathering thickness; (b) P-wave, variable weathering thickness; (c) PS-wave, constant weathering thickness; (d) PS-wave, variable weathering thickness. PS time axes have been scaled such that sections have approximately the same depth extent.

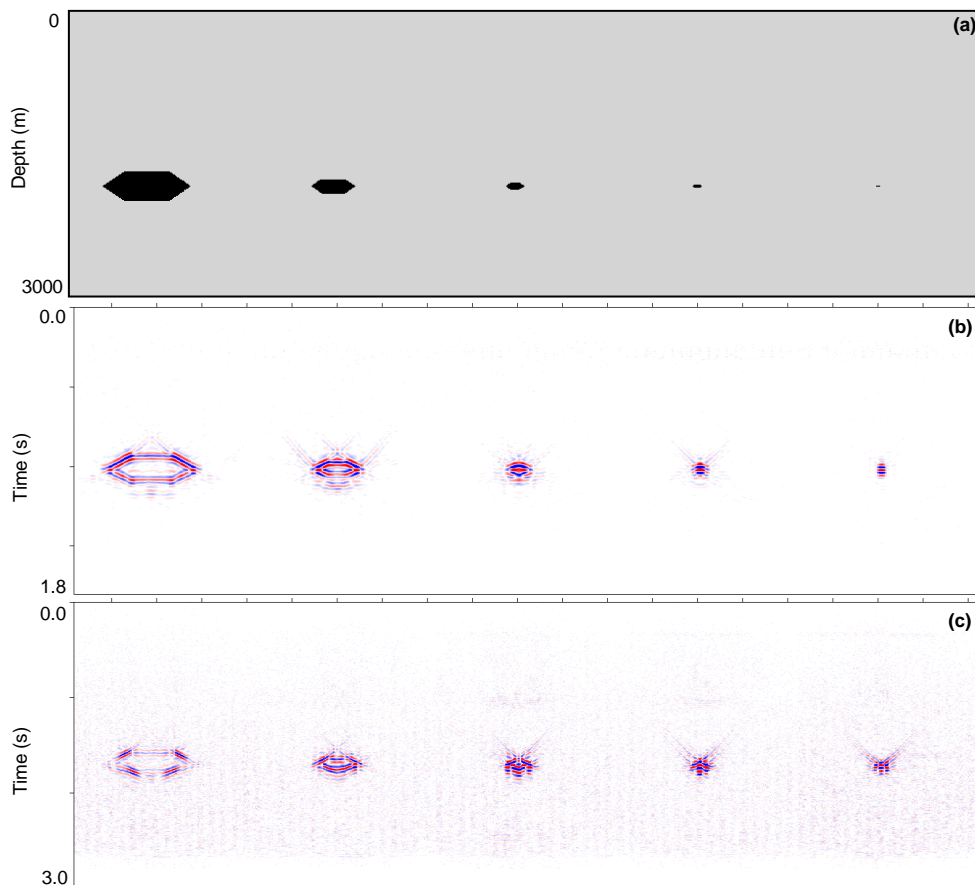


Figure A2. (a) Petroleum scale model representing sand lenses of various dimensions. The target sand lens' are centred at 1850m with overall extents of 1000x300m, 500x150m, 200x60m, 100x30m, and 50x15m. (b) Corresponding P-wave image. (c) PS-wave image.